Advances in Science and Technology Research Journal

Advances in Science and Technology Research Journal, 18(7), 419–436
https://doi.org/10.12913/22998624/193862
ISSN 2299-8624, License CC-BY 4.0

Received: 2024.09.11
Accepted: 2024.09.25
Published: 2024.10.06

An Adaptive Predictor-Based Control Approach for Tracking Control of a Hydraulic Actuator System

Dao Thanh Liem[1], Nguyen Minh Huy[1], Le Van Nam[1], Ho Thi My Nu[1*]

[1] Faculty of Mechanical Technology, Ho Chi Minh City University of Industry and Trade, 140 Le Trong Tan, Ho Chi Minh City, Vietnam

* Corresponding author's e-mail: nuhtm@huit.edu.vn

ABSTRACT

Electro-hydraulic actuators offer advantages over traditional hydraulic actuators, particularly for high-precision force or position control, but their nonlinear dynamics complicate modelling and control. This study proposes a predictor-integrated adaptive controller to address these challenges. By combining a proportional-integral-derivative controller with a sliding surface, the system tracks desired trajectories, while a parameter optimization rule minimizes errors. Additionally, a smart grey prediction model with dynamic step size adjusts parameters and generates control signals to reduce noise and disturbances. Simulations show improved accuracy and control performance, with a root mean square error reduction of over 50% compared to traditional control algorithms. This adaptive approach ensures precise control in varying conditions, making it suitable for aerospace, automotive, and robotics applications.

Keywords: power hydraulics, adaptive control, electro-hydraulic actuator, grey predictor, system modelling.

INTRODUCTION

In the last decades, hydraulic systems are extensively employed in both industrial and mobile applications due to their solidity, superior power-to-mass ratio, and rapid feedback times. Recent research on hydraulic systems has led to advancements in parametric identification, trajectory tracking, fault detection, and state estimation to enhance control performance [1–5]. In general, valve-controlled hydraulic systems are commonly used because of their high power-to-size ratio. However, they suffer from low energy efficiency caused by energy dissipation through pump bypass leaks and throttle losses at control valves. These systems also present challenges such as environmental concerns from fluid leaks, high maintenance demands, substantial weight, and spatial constraints during installation [6-8]. To address these issues, various advancements have been made in hydraulic engineering. A model for a hydraulic system featuring an asymmetric cylinder driven by a directional valve, incorporating a variable bulk modulus, was developed to addresses the position control [9]. A friction model that accounts for the friction-velocity relationship, consisting of Coulomb-Stribeck friction, was introduced to perform force tracking control of an electro-hydraulic actuator (EHA) [10]. Internal leakage within the servo valve and actuator was emphasized in the application of a fuzzy logic position control [11], while the position control of an electro-hydraulic servo system characterized by a asymmetric and large dead zone was examined considered factors such as time variability, dead zone, time lag, and saturation nonlinearity in a servo hydraulic press [12]. These studies provide insights into addressing nonlinearities in hydraulic system modelling. One other promising alternative gaining attention is EHA systems. EHA systems, as fundamental parts, and components,

have been used in numerous types of equipment, including construction machinery, agricultural machines, and airplanes [13, 14]. These applications often require high power to perform tasks such as lifting heavy weights or moving materials. The energy for these systems is generally produced by a central source, often an internal combustion engine or a high-capacity electric motor. Fluid power systems enable the efficient transmission of energy through hydraulic lines to linear or rotary actuators. Concurrently, concerns about energy conservation in hydraulic systems have risen with the increased use of heavy equipment [15]. EHA systems frequently run continuously and deliver high power to manage heavy loads, leading to substantial energy usage and exhaust emissions [16]. Thus, even a minor enhancement in hydraulic system efficiency can greatly influence the machine's overall energy efficiency. Each EHA system converts power from high-speed performance of an electric motor to the high-force output of a hydraulic actuator. These systems usually include a reservoir, valves, an electric motor, a bidirectional pump, and an end-effector (such as a linear or rotary actuator) directly driven by the pump. EHA systems provide a more streamlined, eco-friendly, and energy-efficient means of delivering high force, thanks to their superior stiffness compared to valve-controlled hydraulic systems. Achieving precise control of EHAs is challenging due to inherent nonlinearities and uncertainties. Accurate modelling of the controlled plant is fundamental for position control. However, constructing a precise mathematical model for EHA systems is difficult because of their inherent nonlinearity and significant uncertainties [17, 18]. These challenges arise from factors such as flow area dead zones, friction, leakage and fluid compressibility, and the intricate pressure-flow characteristics of control valves. These nonlinearities result from fluid dynamics and hardware interactions, while uncertainties stem from friction and variations in fluid temperature and pressure. Consequently, precision control in EHAs has become a major focus of research.

To manage the complexities of controlling nonlinear systems, various control methodologies have been developed. The conventional proportional-integral-derivative (PID) controller struggles to perform well across different load conditions due to its fixed gains. Despite its simplicity and robust operation, enhancements to the PID algorithm are needed to optimize system response. As a result, there is growing interest in integrating innovative control methods with traditional approaches to improve performance. Several hybrid control strategies have been explored, with PID controller combinations being common [19–21]. For instance, integrating a conventional PID controller with an adaptive or robust controller, or combining a robust PID model with an output feedback controller for networked control systems, for example, those governing DC motors, has shown effective in simulation studies. Optimal tuning of PID controllers for velocity and position control in hydraulic systems has led to satisfactory system performance. Various adaptive PID controllers have been developed, such as intelligent PID control, self-tuning PID controllers [22], and online-tuning PID controllers [23], among others. Combining a tuning mechanism with PID control offers considerable potential in control system design, leveraging the simplicity of PID control alongside its capacity to learn, adapt, and manage nonlinearity. Moreover, significant improvements in control performance can be realized by integrating feedforward and feedback control, particularly when large disturbances can be measured in advance before they affect the process output. Ideally, feedforward control can decouple the influence of these measured disturbances on the output. However, its application requires a cost-benefit analysis, as the benefits of disturbance rejection must be weighed against the manufacturing and maintenance costs. Additionally, feedforward control relies on knowledge of the system's mathematical model, the availability of external control signals, and an understanding of how the system output responds to load changes. Consequently, feedforward control does not rely solely on error correction; it also requires a deep understanding of the process model and accurate measurement of the disturbances impacting the system [24]. Additionally, integrating traditional PID control with fuzzy control algorithms has emerged as a promising approach to enhance controller effectiveness and system performance further [25–27]. Fuzzy logic control techniques have been adopted for designing control systems, leveraging linguistic information, particularly useful in velocity control systems for hydraulics due to fuzzy control's model-free nature and robustness.

Implementing the fuzzy logic model involves specific challenges, notably the requirement for intricate learning mechanisms or the trial-and-error construction of performance decision tables [28]. A significant hurdle is the substantial number of fuzzy logic rules required, complicating the evaluation. The effectiveness of the system is contingent on the time invested in implementation and the designer's experience. To address these complexities, methods integrating sliding mode control into fuzzy control systems have been developed. Sliding mode control, known for its effectiveness in managing nonlinear systems and reducing model uncertainty, is well-suited for addressing the inherent nonlinearity in hydraulic systems. Research has demonstrated that integrating sliding mode control with fuzzy logic techniques can enhance performance and robustness while reducing the number of required fuzzy rules. One notable advantage is its ability to function effectively with fewer rules compared to traditional fuzzy control methods, coupled with improved robustness against parameter variations. However, similar to conventional fuzzy control systems, designing rules for fuzzy sliding mode control necessitates prior tuning through trial-and-error, which can be time-consuming.

In response to these challenges, research has focused on developing adaptive fuzzy controllers using the Lyapunov synthesis approach [29]. These controllers automatically adjust fuzzy rules to achieve satisfactory system responses. However, they require prior knowledge of the plant during the design phase, and the extensive number of rules may limit their applicability in certain scenarios. Grey model has emerged as a preferred solution, facilitating the collection of system process and disturbance data [30, 31]. Grey prediction methodologies can accurately forecast system outputs without requiring a comprehensive understanding of the system's mathematical model. The grey prediction framework is particularly suited for systems with unknown parameters and has been widely applied in various engineering challenges.

Therefore, a tailored control solution for the position control of EHA systems is necessary. This study proposes a predictor-integrated adaptive controller, termed the adaptive sliding mode-PID (SMCPID) based on smart grey model (SGP) control approach, named as ASSG, to mitigate EHA system nonlinearities and manage variations in frequency of desired trajectory and load for precise position control. The proposed approach combines adaptive SMCPID methods to reduce reaching time and oscillation through high sliding surface gains. An online fuzzy tuning method adjusts sliding surface gains to mimic those of a PID controller under robust checking conditions. This controller incorporates an adaptive fuzzy control scheme, a SMCPID reaching controller, and a smart grey model adapted from the standard grey prediction model for a first-order single variable. This smart grey model predicts the system's future performance, ensuring the stability of the control parameters within the adaptive controller through rigorous Lyapunov analysis. Moreover, this control strategy effectively addresses parametric uncertainties arising from model variations and disturbances, making it suitable for systems characterized by such uncertainties.

CONTROL ALGORITHM DESIGN

As outlined above, the ASSG is built utilizing an adaptive sliding mode PID (ASPID) controller incorporating a smart prediction model (SGP). In this controller as depicted in Figure 1, the ASPID model is designed to direct the hydraulic system towards predefined trajectories. In addition, a robust verification conditions-based learning mechanism is incorporated with the PID controller to continuously adjust their parameters in real-time, of which the goal is to minimize the control errors. In the meantime, the SGP, endowed with self-tuning capabilities for predictor step size, serves two primary functions: first, it forecasts the system response in next future to proactively optimize the control factors, and second, it generates a compensatory control input in response to the perturbations of the system, thereby enhancing overall control performance.

EHA mathematical model

Considering the EHA system depicted in Figure 2, the piston dynamics can be represented by:

$$m\ddot{y} = P_H A_H - P_R A_R - F \tag{1}$$

where: m, k, c represent the equivalent mass, stiffness, and damping, respectively; y is the displacement of the system; PH, PR are the pressures in the two chambers; AH, AR are the respective actuating areas; and F is the external load force.

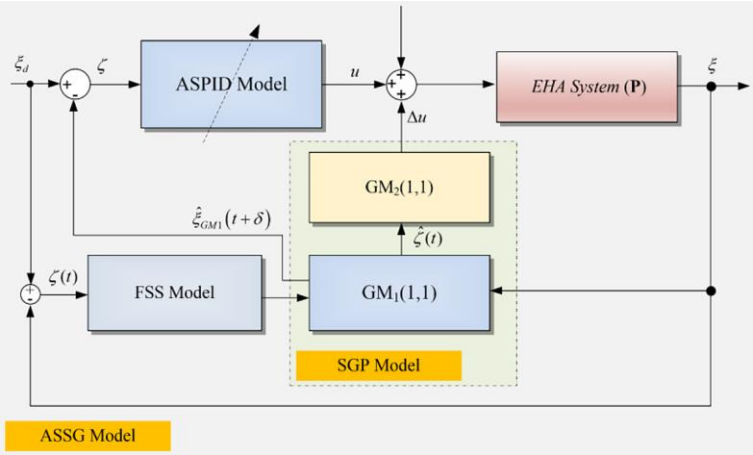

Figure 1. The structure of ASSG control model

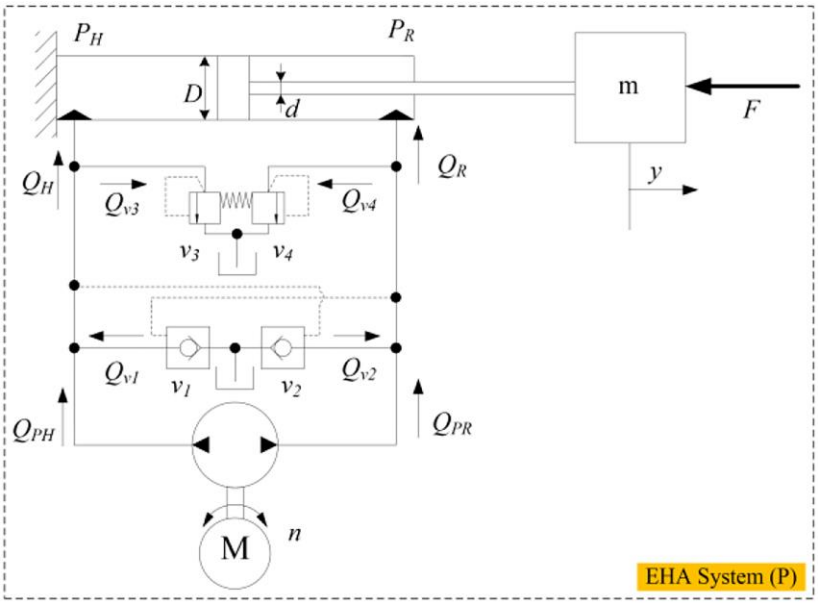

Figure 2. The structure of the EHA system

Assuming no external leakage, the dynamics of the cylinder oil flow can be expressed as:

$$\begin{cases} \dot{P}_H = \dfrac{\beta_e}{V_{01} + A_H y}\left(Q_H - A_H \dot{y} - C_t\left(P_H - P_R\right)\right) \\ \dot{P}_R = \dfrac{\beta_e}{V_{02} - A_R y}\left(Q_R + A_R \dot{y} + C_t\left(P_H - P_R\right)\right) \end{cases} \tag{2}$$

where: C_t is the internal leakage coefficient of the cylinder, β_e is the effective bulk modulus of the hydraulic fluid, and V_{01}, V_{02} represent the initial total control volumes of the two chambers (including pipeline and initial cylinder chamber volumes). Q_H and Q_R denote the flow rates into the H chamber (cylinder end) and R chamber (rod end), respectively.

The flow rates for both chambers are calculated as:

$$\begin{cases} Q_H = Q_{PH} + Q_{v1} - Q_{v3} \\ Q_R = Q_{PR} + Q_{v2} - Q_{v4} \end{cases} \tag{3}$$

where: $Q_{PH} = -Q_{PR} = Q_{pump}$ represents the flow rate supplied by the pump:

$$Q_{pump} = D\omega - k_{leakage}\left(P_H - P_R\right) \tag{4}$$

where: $k_{leakage}$ denotes the leakage constant, D represents the pump displacement, and ω is the input drive speed from the servo system. Assuming the pressure in the oil tank is negligible ($P_{tank} = 0$), the terms Q_{v1}, Q_{v2}, Q_{v3}, and Q_{v4} correspond to the flow rates through valves v_1, v_2, v_3, and v_4, respectively.

ASPID control model design

Let's start by analyzing the following general system:

$$\begin{cases} \dot{\xi}_1(t) = \xi_2(t) \\ \dot{\xi}_2(t) = F(\xi_1(t), \xi_2(t), u(t)) \\ \varsigma(t) = \xi_1(t) \end{cases} \tag{5}$$

where: $\xi = (\xi_1, \xi_2, \ldots, \xi_n)^T \in \Re^n$ represents the the system's input vector, the control signal depicted by $u \in \Re^m$, F: $\Re^{n\times m} \to \Re^n$, and $\varsigma \in \Re^r$. Let $\zeta(t)$ be the difference between the reference signal ξ_d and the system response ξ ,

$$\zeta(t) = \xi_d(t) - \xi(t) \tag{6}$$

Define the reference signal as indicated below:

$$\dot{\xi}_r(t) = \ddot{\xi}_d(t) + c_1\dot{\zeta}(t) + c_0\zeta(t) \tag{7}$$

where: the coefficients c_1 and c_0 are determined to ensure that the roots of $s^2 + c_1 s + c_0 = 0$ within the left-half of the complex plane. The following manner defines the sliding mode surface as:

$$\vartheta(t) = \xi_r(t) - \xi_2(t) \tag{8}$$

When the sliding mode takes place, the ϑ approaches zero, indicating the control error tends to zero when the time approaches infinity. Combining Equations 6–8, we obtain the following Equations:

$$\vartheta(t) = \dot{\zeta}(t) + c_0\int \zeta(t)dt + c_1\zeta(t) \tag{9}$$

$$\dot{\vartheta}(t) = \ddot{\zeta}(t) + c_0\zeta(t) + c_1\dot{\zeta}(t) \tag{10}$$

Here, the reference signal allows the control model to increase the sliding surface level, enabling the achievement of an integral sliding surface that ensures stability. Moreover, the sliding surface converges to zero, thereby improving the control efficiency. The Lyapunov function can be defined as the following:

$$V(t) = \frac{1}{2}\vartheta^2(t) = (\xi_r(t) - \xi_2(t))^2 \tag{11}$$

and its derivative:

$$\dot{V}(t) = \dot{\vartheta}(t)\vartheta(t) = (\dot{\zeta}(t) + c_0\int \zeta(t)dt + c_1\zeta(t))(\ddot{\zeta}(t) + c_0\zeta(t) + c_1\dot{\zeta}(t)) \tag{12}$$

The terms $\dot{\zeta}(t), \zeta(t)$ and their integrals/derivatives form a quadratic expression in $\zeta(t)$ and its derivatives. Typically, if damping is present (i.e., the system has terms proportional to $\zeta(t)$ or its derivatives, like the c_0 and c_1 terms), these quadratic terms lead to non-positive derivatives for Lyapunov functions. The term $\dot{\zeta}(t) + c_0\int \zeta(t)dt + c_1\zeta(t)$ represents a combination of the error, its rate of change, and an integrated term. These typically contribute to stabilizing the system (i.e., driving $\zeta(t)$ to zero). The second term $\ddot{\zeta}(t) + c_0\zeta(t) + c_1\dot{\zeta}(t)$ adds further dynamics that should also help dampen the system. For $\dot{V}(t)$ to be non-positive, constants c_0 and c_1 need to be carefully chosen. If both c_0 and c_1 are

positive, they contribute damping to the system and help ensure that the error $\zeta(t)$ (or $\vartheta(t)$) decreases over time. Hence, the error $\vartheta(t)=\zeta(t)$ tends to zero, ensuring stability. To attain system stable, the control signal output is produced to satisfy the equation bellow:

$$\dot{\vartheta}(t) = -c\, sgn(\vartheta(t)) \tag{13}$$

where:

$$\text{sgn}(\vartheta(t)) = \begin{cases} -1\,;\vartheta(t)<0 \\ 0\;\;;\vartheta(t)=0 \\ 1\;\;;\vartheta(t)>0 \end{cases} \tag{14}$$

In this context, the control signal is divided into two components:

$$u(t)=u_{sw}(t)+u_{eq}(t) \tag{15}$$

In Equation 15, the sliding mode control output, $u_{sw}(t)=\alpha csign\left(\vartheta(t)\right)$, transitions the system to the sliding surface, while α represents the input factor. The control output at the equivalent point, u_{eq}, is obtained as the following:

$$u_{eq}(t)=\alpha\left(\dot{\xi}_r(t)-F(t)\right)\approx u_{PID}=k_P\zeta(t)+k_I\int\zeta(t)dt+k_D\frac{d\zeta(t)}{dt} \tag{16}$$

where: the PID model generates the output to counteract noise and disturbances. To optimize the PID controller parameters, the objective function is selected as bellow:

$$V_o(t)=0.5\left(u_{eq}(t)-u_{PID}(t)\right)^2=0.5\zeta_o^2(t) \tag{17}$$

wherein, the PID controller parameters optimization adhere to the gradient descent technique:

$$k_P\left(t+\Delta t\right)=k_P\left(t\right)+\eta_1\zeta_o\frac{d\zeta_o(t)}{dk_P}=k_P\left(t\right)+\eta_1\zeta_o(t)\zeta(t) \tag{18}$$

$$k_I\left(t+\Delta t\right)=k_I\left(t\right)+\eta_2\zeta_o(t)\frac{d\zeta_o(t)}{dk_I}=k_I\left(k\right)+\eta_2\zeta_o(t)\int\zeta(t)dt \tag{19}$$

$$k_D\left(t+\Delta t\right)=k_D\left(t\right)+\eta_1\zeta_o(t)\frac{d\zeta_o(t)}{dk_D}=k_D\left(t\right)+\eta_3\zeta_o(t)\frac{d\zeta(t)}{dt} \tag{20}$$

In this control structure, if the output of the PID model $u_{PID}(t)\to u_{eq}(t)$, $\zeta_0(t)\to 0$ then $\vartheta(t)\to 0$. Consequently, the parameters of the controller is updated by the following:

$$\begin{cases} k_P\left(t+\Delta t\right)=k_P\left(t\right)+\eta_1\vartheta(t)\zeta(t) \\ k_I\left(t+\Delta t\right)=k_I\left(t\right)+\eta_2\vartheta(t)\int\zeta(t)dt \\ k_D\left(t+\Delta t\right)=k_D\left(t\right)+\eta_3\vartheta(t)\dfrac{d\zeta(t)}{dt} \end{cases} \tag{21}$$

To determine the sliding control gain, we substitute the value of with the saturation value as follows:

$$sat\left(\vartheta/\beta\right)=\begin{cases} 1 \;\; ; & \vartheta/\beta>1 \\ -1 \;\; ; & \vartheta/\beta<-1 \\ \vartheta/\beta\,; & others \end{cases} \tag{22}$$

where: β represents the width of the boundary layer. Then, the sliding mode control output is obtained as bellow:

$$u_{sw} = \alpha_{\max} ksat(s/\beta) = k_{\max} sat(s/\beta) \tag{23}$$

To ensure the stability of the control approach, the robust adjustment algorithms for the gains are implemented. Robust control methodology encompasses two main objectives: ensuring closed-loop equilibrium, validated with adequate allowances, and achieving suppression of closed-loop disturbances. To realize these objectives, the parameters of the PID controller are determined according to robust control criteria. To stabilize the control system, it is crucial to uphold a gain margin of around 3 dB for the feedback control system.

SGP model implementation

In this control algorithm, the SGP model serving two main functions: to predict the system output to guide the ASPID model and to compensate for system feedback deviations caused by environmental noise and disturbances during subsequent operation. The grey prediction method utilized by the $GM_1(1,1)$ model follows these steps. Firstly, the n output data ($n \geq 4$) are necessary to approximate a system which can be obtained as the following:

$$\xi_{GM1}^{(0)} = \{\xi_{GM1}^{(0)}(t_k - n + 1), \xi_{GM1}^{(0)}(t_k - n + 2), ..., \xi_{GM1}^{(0)}(t_k)\}; \tag{24}$$

The next step of the $GM_1(1,1)$ modelling procedure involves calculating $\xi^{(1)}$ from $\xi^{(0)}$ using the accumulated generating operation:

$$\xi_{GM1}^{(1)}(t_k) = \sum_{i=1}^{t_k} \xi_{GM1}^{(0)}(i); (t_k : t - n + 1, t - n + 2, ..., t) \tag{25}$$

Then, a adjacent neighbour of $\varsigma^{(1)}$ from $\xi^{(1)}$ can be produced by the mean generating operation as bellow:

$$\varsigma_{GM1}^{(1)}(t_k) = \frac{1}{2}\left(\xi_{GM1}^{(1)}(t_k) + \xi_{GM1}^{(1)}(t_k - 1)\right) \tag{26}$$

The next step of the modelling process involves obtaining the differential equation of the first grey model, $GM_1(1,1)$ as the following:

$$\xi_{GM1}^{(0)}(t_k) + \tau_1 \varsigma_{GM1}^{(1)}(t_k) = \rho_1 \tag{27}$$

where: the least squares method is used to establish the parameter $[\tau_1, \rho_1]$. Particularly, the least squares method can be executed as follows:

$$\hat{\tau}_1 = \begin{bmatrix} \tau_1 \\ \rho_1 \end{bmatrix} = \left(D_1^T D_1\right)^{-1} D_1^T E_1 \tag{28}$$

$$D_1 = \begin{bmatrix} -\varsigma_{GM1}^{(1)}(2) & 1 \\ -\varsigma_{GM1}^{(1)}(3) & 1 \\ \vdots & \vdots \\ -\varsigma_{GM1}^{(1)}(t_k) & 1 \end{bmatrix}; \quad E_1 = \begin{bmatrix} \xi_{GM1}^{(0)}(2) \\ \xi_{GM1}^{(0)}(3) \\ \vdots \\ \xi_{GM1}^{(0)}(t_k) \end{bmatrix} \tag{29}$$

The final step of the process involves obtaining the prediction model:

$$\hat{\xi}_{GM1}^{(1)}(t_k + 1) = \left(\xi_{GM1}^{(1)}(1) - \frac{\rho_1}{\tau_1}\right) e^{-at_k} + \frac{\rho_1}{\tau_1} \tag{30}$$

$$\hat{\xi}_{GM1}^{(0)}(t + \delta) = \hat{\xi}_{GM1}^{(1)}(t + \delta) - \hat{\xi}_{GM1}^{(1)}(t + \delta - 1) \tag{31}$$

The performance of a prediction model employing a grey predictor depends directly on the predictor step. At the beginning, the SGP design includes a grey predictor with a fixed step size. Nonetheless, it's clear that a smaller step size speeds up the system actuation but results in greater oscillation and/or overshoot. In contrast, the overshoot or oscillation can be reduced by a larger predictor step size, but it leads to the increase the system's rise time. Therefore, an adaptive predictor step size is suitable to mitigate these limitations. Additionally, an evaluation factor is defined to determine the current step extent. This considers both the prior and the next steps to ascertain if the predicted value is sufficient to enhance the performance of the control approach. The step size of the prediction model is derived as the following Equation:

$$\delta(t_k+1)=\gamma(t_k+1)\delta(t_k)+(1-\gamma(t_k+1))\delta_{AS}\left(t_k+1\right) \tag{32}$$

Here, two fuzzy sets are employed to produce the δ_{AS} and γ(t) in Equation 32. The triangle membership functions (TMFs) is employed in the adaptive prediction step (APS) fuzzy. The inputs are depicted by seven TMFs (LN, MN, SN, Z, SP, MP, and BP) mean (Large, Medium, Small Negative, Zero, Small, Medium, and Big Positive). On the other hand, five TMFs represent the output of the fuzzy set as: ES, S, M, L, and EL (mean Extra Small, Small, Medium, Large", and Extra Large). Figure 3 illustrates the shapes and positions of the membership functions of the input and output. The fuzzy rules for the APS are obtained in Table 1 utilizing the IF-THEN configuration based on the aforementioned fuzzy sets of the input and output variables.

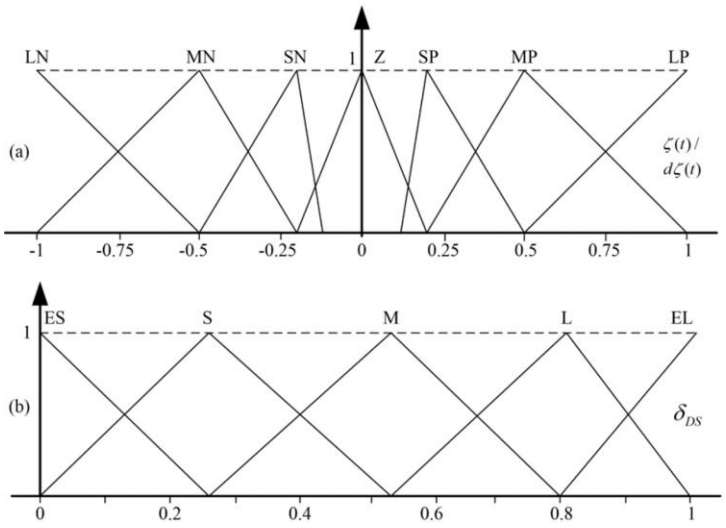

Figure 3. Fuzzy step size model, (a) MFs of fuzzy inputs (b) MFs of fuzzy output

Table 1. Fuzzy rule table for the APS

Step size		Input 2						
		LN	MN	SN	Z	SP	MP	LB
Input 1	LN	EL	EL	L	M	ES	ES	ES
	MN	EL	L	M	S	ES	ES	ES
	SN	EL	L	M	S	S	S	M
	Z	EL	L	M	M	L	L	EL
	SP	M	S	S	S	L	EL	EL
	MP	ES	ES	S	S	L	EL	EL
	LP	ES	ES	ES	S	EL	EL	EL

Besides, there are two inputs and one output in the adaptive evaluation factor (AEF). The inputs are depicted by three TMFs: N, Z, and P (mean Negative, Zero and Positive). On the other hand, four membership functions are employed as: ES, S, M and L (mean Extra Small, Small", Medium, and Large) for the output. Figure 4 displays the shapes and positions of the input and output membership functions. Using the aforementioned fuzzy sets of input and output variables, the fuzzy rules for the AEF are documented in Table 2 utilizing the IF-THEN format.

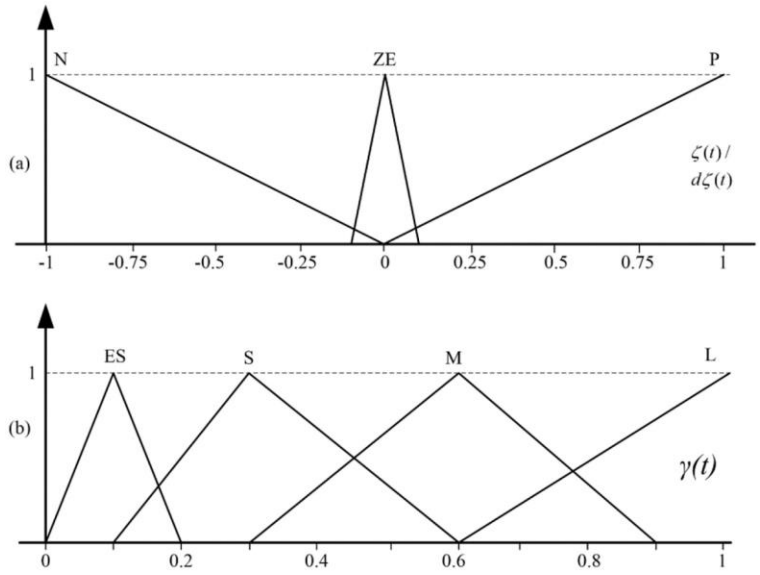

Figure 4. Fuzzy step size (a) MFs of adaptive evaluation factor inputs (b) MFs of fuzzy output

Table 2. Fuzzy rule table for the AEF

Evaluating factor		Input 2		
		N	Z	P
Input 1	N	ES	S	ES
	Z	M	L	M
	P	ES	S	ES

The purpose of employing the second grey model, $GM_2(1,1)$, is to estimate the impact of the noise and disturbances in the subsequent step, aiming to generate an appropriate compensatory signal. Consequently, the construction process of the prediction model $GM_2(1,1)$ closely resembles that of the first grey prediction model, with the distinction lying in the input used. In this design, the gathered input data reflects the response to disturbances and noise of the system, denoted as:

$$\zeta_{GM2}^{(0)} = \left\{ \zeta_{GM2}^{(0)}(1), \zeta_{GM2}^{(0)}(2), \ldots, \zeta_{GM2}^{(0)}(m) \right\} \tag{33}$$

where:

$$\zeta_{GM2}^{(0)}(k) = \xi^{(0)}(k) - \hat{\xi}^{(0)}(k); (k = 1,2,...,m) \tag{34}$$

The mean generating operation is applied

$$\varsigma_{GM2}^{(1)}(t_k) = \frac{1}{2}\left(\xi_{GM2}^{(1)}(t_k) + \xi_{GM2}^{(1)}(t_k - 1) \right) \tag{35}$$

$$\zeta_{GM2}^{(0)}(t_k) + \tau_2 \varsigma_{GM2}^{(1)}(t_k) = \rho_2 \tag{36}$$

where: the least squares method is used to establish the parameter $[\tau_2, \rho_2]$. Particularly, the least squares method can be executed as follows:

$$\hat{\tau} = \begin{bmatrix} \tau_2 \\ \rho_2 \end{bmatrix} = \left(D_2{}^T D_2 \right)^{-1} D_2{}^T E_2 \tag{37}$$

$$D_2 = \begin{bmatrix} -\varsigma^{(1)}_{GM_2}(2) & 1 \\ -\varsigma^{(1)}_{GM_2}(3) & 1 \\ \vdots & \vdots \\ -\varsigma^{(1)}_{GM_2}(t) & 1 \end{bmatrix}; \qquad E_2 = \begin{bmatrix} \zeta^{(0)}_{GM2}(2) \\ \zeta^{(0)}_{GM2}(3) \\ \vdots \\ \zeta^{(0)}_{GM2}(t) \end{bmatrix} \tag{38}$$

The final step of the process involves obtaining the prediction model:

$$\hat{\zeta}^{(1)}_{GM2}(t_k+1) = \left(\zeta^{(1)}_{GM2}(1) - \frac{\rho_2}{\tau_2} \right) \mathrm{e}^{-at_k} + \frac{\rho_2}{\tau_2} \tag{39}$$

$$\hat{\zeta}^{(0)}_{GM2}(t_k+1) = \hat{\zeta}^{(1)}_{GM2}(t_k+1) - \hat{\zeta}^{(1)}_{GM2}(t_k) \tag{40}$$

By employing the $GM_2(1,1)$, the output response to the perturbations and noises of the system in the next step can be obtained. Consequently, the additive signal output of the controller for the coming disturbance is denoted as:

$$\Delta u(t+1) \equiv \Delta\hat{\xi}(t+1) = k_{SG} \times \hat{\zeta}^{(0)}_{GM2}(n+1); \tag{41}$$

where: k_{SG} represents an additive gain.

SYSTEM EVALUATION SETUP

In order to implement and evaluate the designed control approach, a system integrating an EHA is set up utilizing co-simulation platform based on Amesim and Matlab/Simulink with an ODE solver. Figure 5 depicts the structure of the evaluate system. In this study, the particular EHA is implemented using the Amesim software, consisting of a pump, a cylinder, and additional valve system. The specification of the system is presented in Table 3. Here, the motor speed controlled the translation of the hydraulic actuator. Additionally, various loads are applied to the system using a pneumatic cylinder connected in series to the hydraulic cylinder rod, with a mass capable of adjusting the friction parameter. Furthermore, a linear scale monitored the motion of the actuators, while a force transducer is used to measure the force generated by the system. As a result, the designed control approach is implemented in the Matlab/Simulink environment to evaluate the controller's performance.

VALIDATION RESULTS

Based on the above setup, the efficiency of the ASSG control model is evaluated in this section. To evaluate the system's robustness the disturbances is generated during the operation. Furthermore, to introduce perturbations, a white noise and sine wave noise was incorporated in the system. Additionally, a comparative evaluation is carried out to assess the effectiveness of the designed ASSG model in comparison to three control model: the traditional PID controller, the fuzzy PID (FPID) controller, the SMCPID. Firstly, simulations evaluated the system's output which respect to a sinusoidal trajectory, with results shown in Figures 6–10. Initially, the PID controller demonstrated significant oscillations and errors, attributed to fixed gains (short-dashed purple lines). The system also showed sluggish and unstable responses during peak activity. Figure 6 displays the PID controller's position responses, while Figure 7 shows the corresponding tracking errors with the same line style.

Subsequently, the control method utilizing FPID is applied to evaluate performance, using the same reference and noise as the PID assessment. However, improvements were limited by the fuzzy set's ability to handle diverse operational conditions. The FPID controller (dash-dotted green line in Figure 6) showed better position tracking than the PID controller, but control errors remained unsatisfactory (Fig. 7, same line style). Furthermore, the SMCPID controller is implemented to assess the

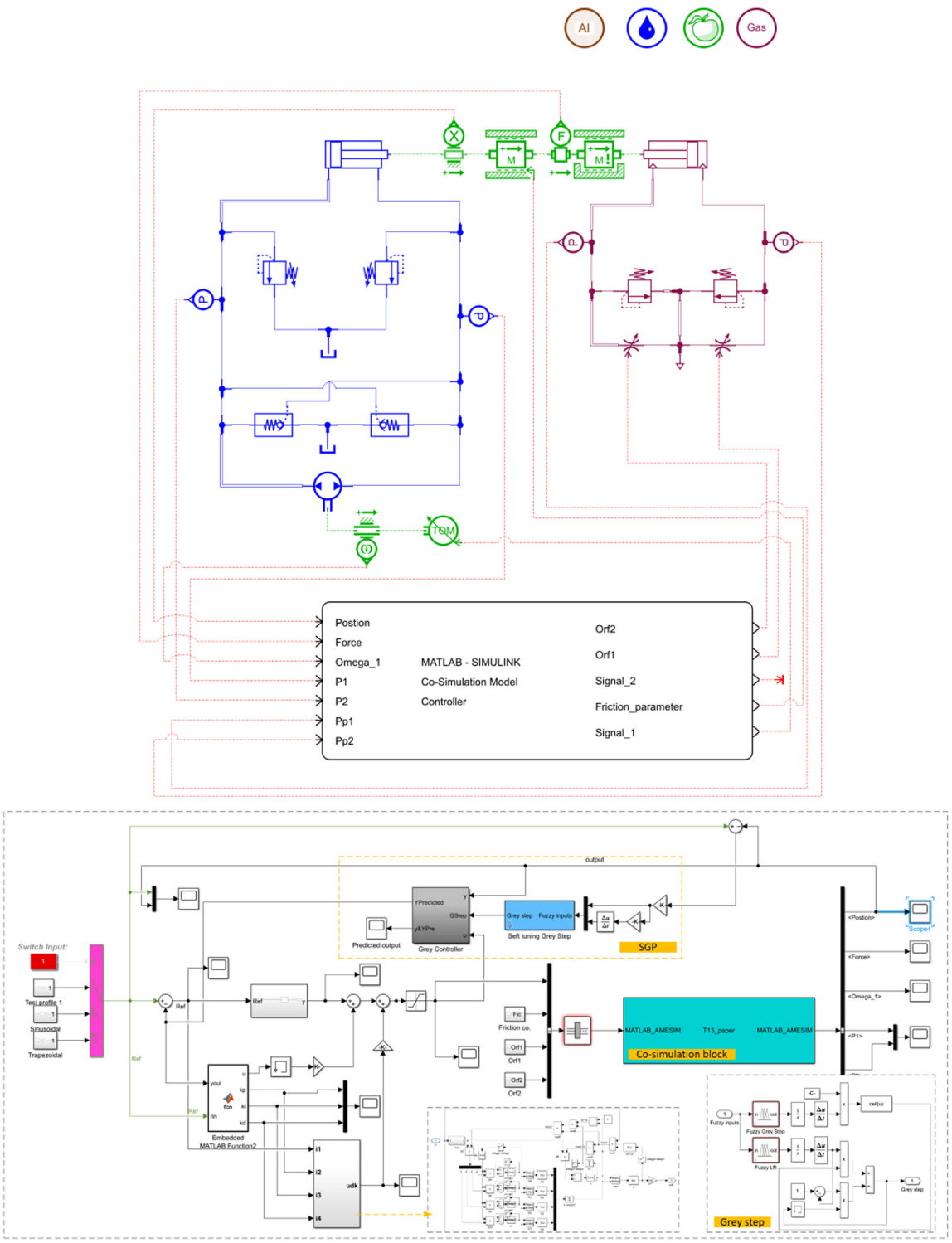

Figure 5. Schematic diagram of the EHA system in co-simulation platform

performance. As depicted in Figure 6, the SMCPID controller demonstrated improved effectiveness compared to other methods, represented by the dotted blue line. However, with significant noise and disturbances, the response of the system produces oscillations, the errors is deemed unacceptably large, as shown by the same line style in Figure 7.

To tackle the control challenges mentioned earlier, the ASSG controller outlined in Section 2 is applied to the system. The trajectory tracking results for the sinusoidal reference are shown by the dashed red line in Figure 6, with the corresponding error represented in Figure 7 using the same line style. These findings illustrate that the

Table 3. System configuration

Device		Specification	
Name	Model		
Hydraulic cylinder	HJ020	Length of stroke	0.5 m
		Piston diameter	0.025 m
		Rod diameter	0.0125 m
Hydraulic relief valve	RV010	Cracking pressure	150 bar
		Flowrate pressure gradient	500 L/min/bar
Hydraulic check valve	CV005	Cracking pressure	1.5 bar
		Flowrate pressure gradient	50 L/min/bar
Hydraulic pump	PU001	Displacement	100 cc/rev
		Typical speed	1000 rev/min
Mass M	MECFR1TK0	Mass	10 kg
Mass friction	MAS010RT	Contact stiffness	200 N/mm
		Coefficient of viscous friction	1000 N/(m/s)
Pneumatic cylinder	PNJ0001	Length of stroke	0.5 m
		Piston diameter	0.025 m
		Rod diameter	0.0125 m
Pneumatic relief valve	PNRV00	Cracking pressure	5 bar
Modulated pneumatic orifice	PNVO001	Flow coefficient setting	0~1

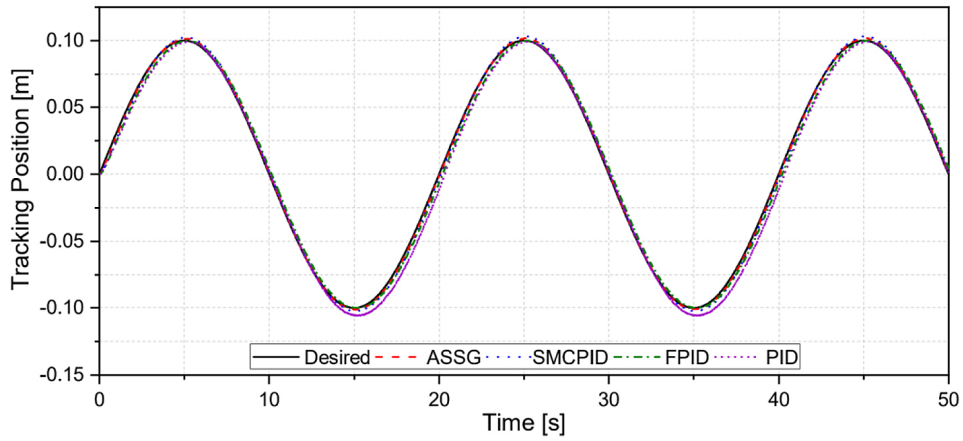

Figure 6. Comparison of trajectory tracking control performance for a sinusoidal reference by using different controllers

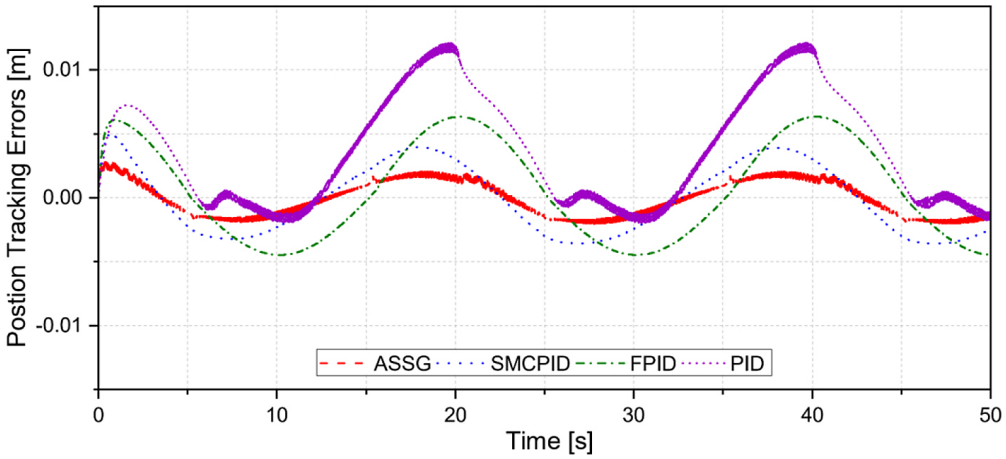

Figure 7. Comparison of trajectory tracking errors for a sinusoidal reference by using different controllers

ASSG control model consistently performs better than those of other control method by delivering faster, highly accurate, and stable system responses. The speed of the motor that drives the pump of the hydraulic system is depicted in Figure 10. The ASSG controller achieves this by leveraging the strengths of the ASPID controller and the SGP predictor. The prediction errors of the SGP for system responses are illustrated in Figure 8 and the PID parameters are indicated in Figure 9

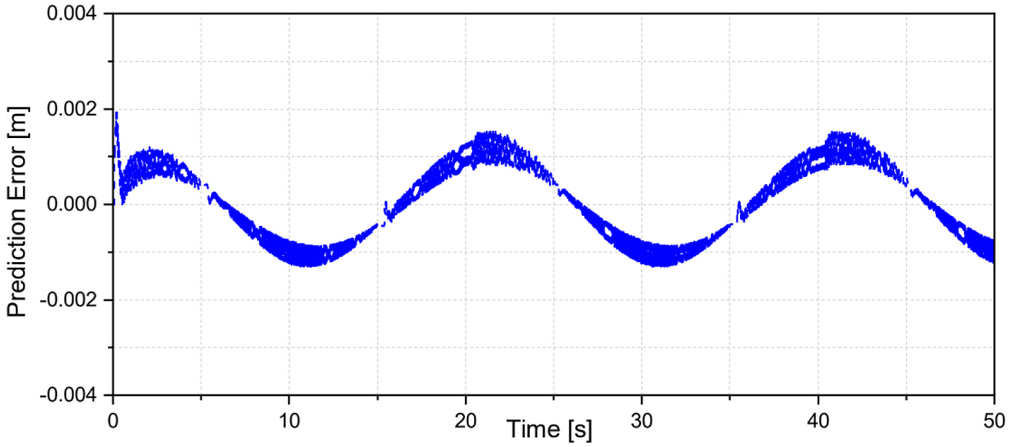

Figure 8. SGP prediction error for a sinusoidal reference by using the ASSG controller

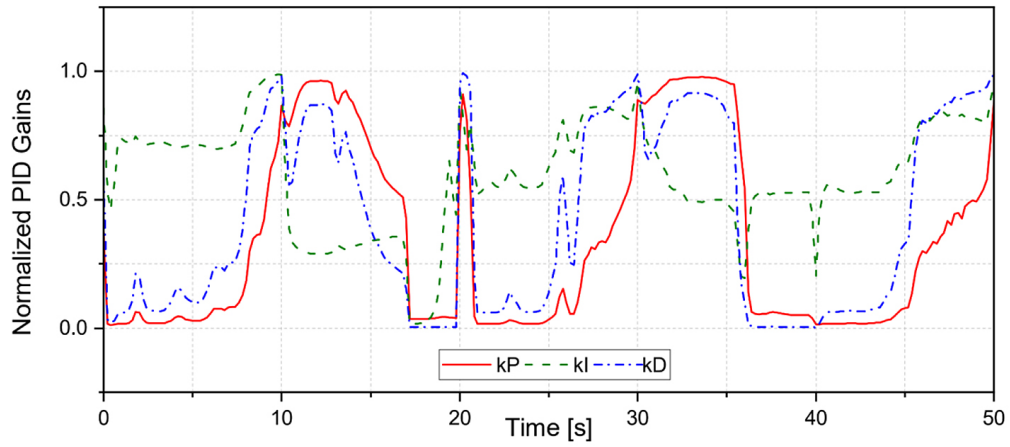

Figure 9. The PID controller parameters for a sinusoidal reference by using the ASSG controller

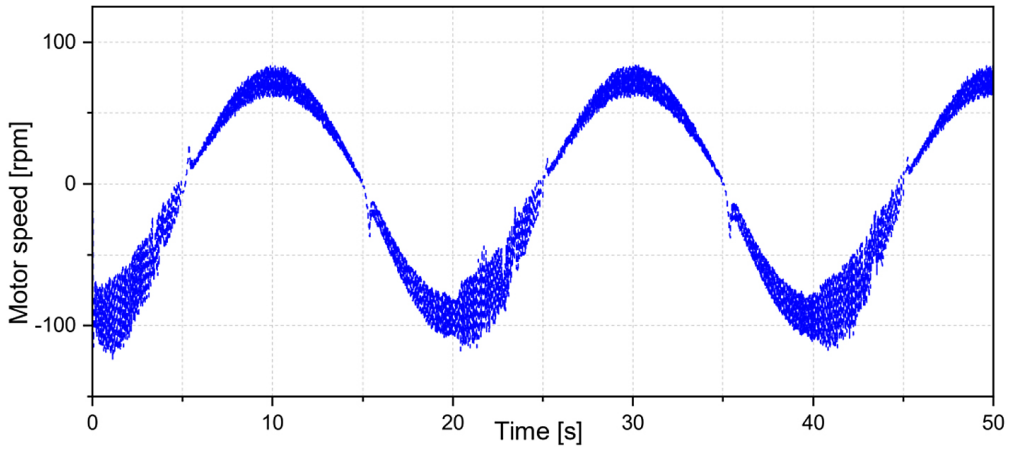

Figure 10. The speed of motor employed in the system for a sinusoidal reference by using the ASSG controller

while the load condition for all evaluation case is shown in Figure 11. Furthermore, the ASSG controller effectively mitigates the negative impacts of disturbances and noise by implementing compensatory control actions generated by the SGP. As seen in the figures, the ASSG controller consistently outperformed other controllers (PID, FPID, SMCPID) in terms of speed, precision, and stability, particularly under disturbances and noise. This demonstrates its robustness and adaptability in varying operational conditions. The ASSG controller integrates the ASPID with a the SGP, allowing for real-time parameter optimization and proactive control adjustments. This combination enhances the controller's ability to mitigate oscillations and control errors effectively. The SGP's self-tuning capabilities enable it to forecast system responses and generate compensatory control inputs, which significantly improve overall control performance. This mechanism ensures that the controller can adapt to parametric uncertainties and maintain precise tracking of predefined trajectories. Consequently, the proposed ASSG controller significantly enhances precise tracking performance.

Subsequent simulations focused on position control using trapezoidal trajectory which is applied in most applications of industrial motion control with various controllers, as depicted in Figures 12–16. The PID control method, represented by the short-dashed purple line, exhibited unstable performance in periods of heightened activity. Besides, the FPID controller, shown by the dash-dotted green line in both figures, demonstrated improved efficiency with respect to those of the PID controller. However, control errors observed with the FPID controller for trapezoidal trajectories were considered unsatisfactory. Furthermore, the SMCPID controller, illustrated by the dotted blue line, outperformed traditional

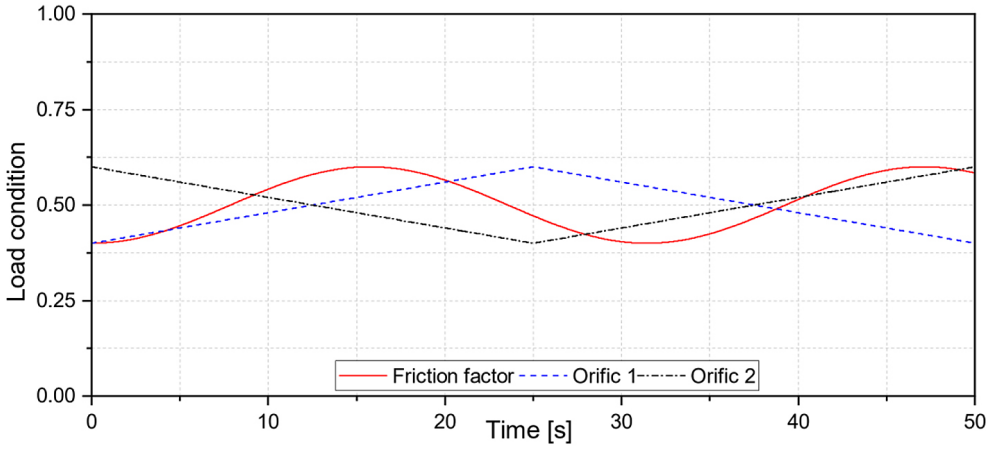

Figure 11. The load condition corresponds to the evaluations

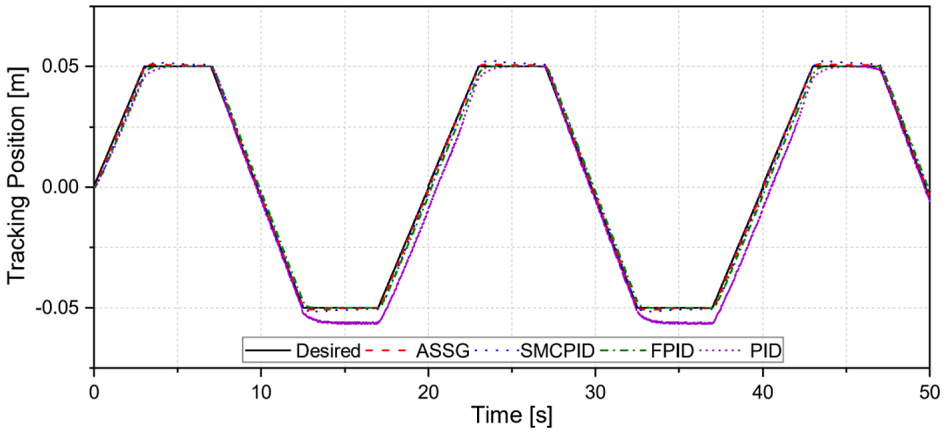

Figure 12. Comparison of trajectory tracking control performance for a trapezoidal reference by using different controllers

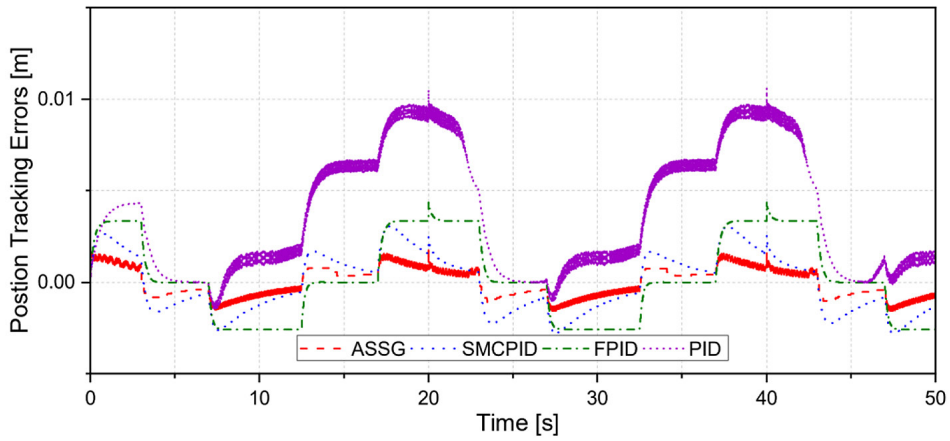

Figure 13. Comparison of trajectory tracking errors for a trapezoidal reference by using different controllers

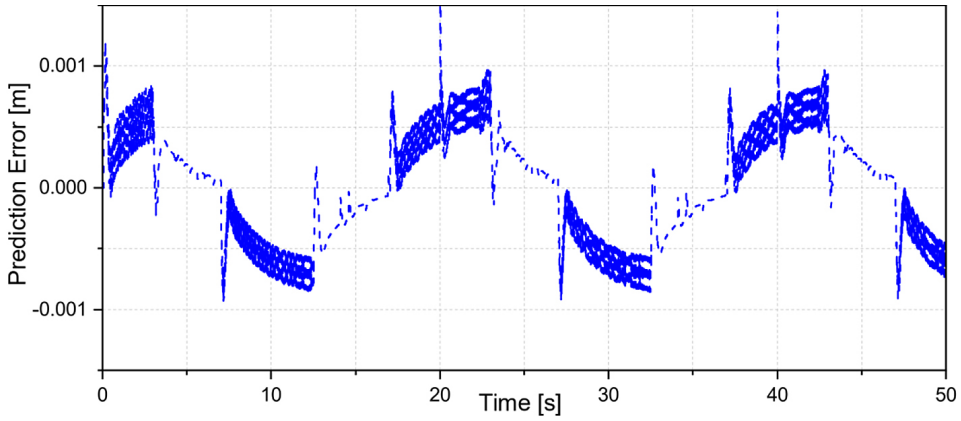

Figure 14. SGP prediction error for a trapezoidal reference by using the ASSG controller

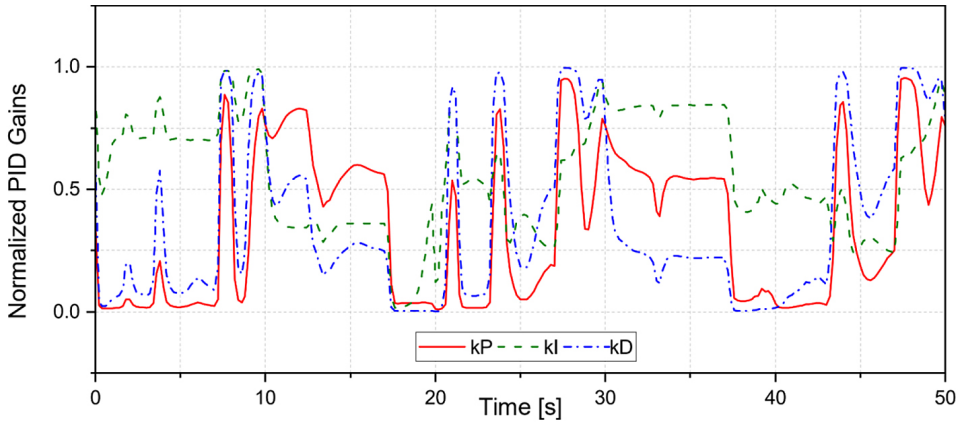

Figure 15. The PID controller parameters for a trapezoidal reference by using the ASSG controller

methods. Despite this, the system's actuation showed oscillations and experienced excessively high errors in certain regions, particularly under disturbance and noise impacts. Both the FPID and SMCPID controllers faced challenges in effectively controlling the system, as indicated by the short-dotted cyan and short-dashed purple lines in Figures 12–13. These controllers exhibited oscillatory responses and unacceptable error levels, especially under significant noise and disturbance conditions. Conversely, the results from the trapezoidal trajectory simulations conclusively demonstrate that the ASSG controller consistently performs better efficiency than those of other

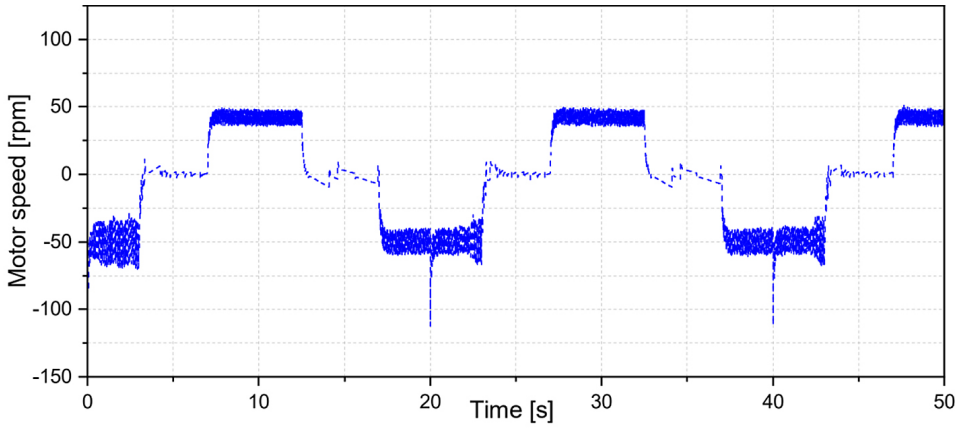

Figure 16. The speed of motor employed in the system for a trapezoidal reference by using the ASSG controller

Table 4. Control performance evaluation

Validation		Evaluation criteria	
Case	Controller	RMSE [m]	ARE [%]
Sinusoidal	PID	0.006342	0.4885
	FPID	0.003605	0.3140
	SMCPID	0.002719	0.2432
	ASSG	0.001345	0.1198
Trapezoidal	PID	0.006105	0.5019
	FPID	0.002584	0.2044
	SMCPID	0.001841	0.1612
	ASSG	0.000901	0.0798

controllers. The system's responses were notably faster, more precise, and exhibited superior stability compared to alternative control methods. The speed of the motor that drives the pump of the hydraulic system is depicted in Figure 16. Figure 14 illustrates the effective predictive capability of SGP in relation to the system's response, along with visual representation of the corresponding prediction errors and the PID controller parameters are indicated in Figure 15.

Furthermore, the performance of the controllers are analyzed in Table 4 using the evaluation criterias: root mean square error (RMSE) and average relative error (ARE) which are defined as Equations 42–43, respectively.

$$\mathrm{RMSE} = \sqrt{\frac{1}{n}\sum_{k=1}^{n}\left(y_{in}(k) - y_{out}(k)\right)^2} \quad (42)$$

$$\mathrm{ARE} = \frac{1}{n}\sum_{k=1}^{n}\left(\frac{|y_{in}(k)-y_{out}(k)|}{y_{in}(k)} \times 100\right)[\%] \quad (43)$$

It is clear that the ASSG controller demonstrated superior efficiency compared to traditional controllers, achieving faster response times and reduced tracking errors. This advantage is particularly evident in its ability to maintain stability and accuracy even under significant disturbances and noise. The combination of the ASPID controller and the SGP predictor enables the controller to effectively manage the dynamic changes in the system's behavior during trapezoidal motion. The SGP's predictive capabilities facilitate the generation of compensatory control signals that counteract disturbances, enhancing the controller's robustness. By continuously optimizing the control parameters based on real-time feedback, the ASSG controller ensures precise tracking of the trapezoidal reference, minimizing oscillations and control errors throughout the operation.

CONCLUSIONS

This study proposes a predictor-integrated adaptive controller for enhancing position tracking control in hydraulic systems. This adaptive controller combines a PID controller and a sliding surface to guide EHAs along specified trajectories, optimizing parameters to minimize control

errors. Additionally, the dynamic step size of the smart grey prediction model adjusts controller parameters and generates supplementary control signals to attenuate noise and disturbances, thereby improving overall control performance. Simulation results confirm the efficacy of this approach, highlighting superior accuracy and performance compared to existing methods. The adaptive learning of the control model optimizes parameters for varying conditions, while continuous adjustment by the prediction model ensures precise system output estimation. In real-time EHA systems, quick response and precision are essential. The proposed controller's ability to predict system behaviours and adjust its control actions in real time allows it to meet the stringent timing and accuracy requirements of online position tracking. By dynamically tuning the control parameters based on real-time feedback, the ASSG controller is capable of maintaining stable and accurate positioning even under varying operational conditions. This makes it highly feasible for real-time deployments where system dynamics can change rapidly. The proposed approach's scalability and real-time adaptability allow for seamless deployment in electronic control units (ECUs), particularly in industries such as aerospace, automotive, and robotics. This work represents a significant advancement in control technology, offering robust, real-time solutions for complex hydraulic systems.

For future work, several areas could be explored to enhance the proposed controller's performance and extend its applications. First, the integration of advanced machine learning techniques could further improve the adaptive capabilities of the controller, allowing it to better predict and respond to highly dynamic environments and more complex disturbances. Second, hardware-in-the-loop (HIL) testing and real-world implementation on physical systems would be a crucial step in validating the controller's real-time applicability in practical settings, such as aerospace and automotive systems. This would provide insights into the controller's performance under actual operational constraints and help optimize the algorithm for specific ECU hardware. Additionally, expanding the controller's framework to handle multi-input multi-output (MIMO) systems could broaden its range of applications, making it suitable for more complex control problems. Lastly, the exploration of energy efficiency improvements in electro-hydraulic systems through the controller's adaptive and predictive nature could be an important future direction, especially for applications with strict energy constraints.

Acknowledgements

This work was financially supported by Ho Chi Minh City University of Industry and Trade under Contract no 05/HĐ-DCT dated 09 Jan 2024.

REFERENCES

1. Feng H., Jiang J., Chang X., Yin C., Cao D., Yu H., Li C. and Xie J. Adaptive sliding mode controller based on fuzzy rules for a typical excavator electro-hydraulic position control system, Engineering Applications of Artificial Intelligence, 2023, 126, 107008. https://doi.org/10.1016/j.engappai.2023.107008
2. Chen J.J.L., Gao W., Wang C., Xu W., Ai C. and Chen G. Position control for a hydraulic loading system using the adaptive backsliding control method, Control Engineering Practice, 2023, 138, 105586. https://doi.org/10.1016/j.conengprac.2023.105586
3. Phan V.D., Truong H.V.A. and Ahn K.K. Actuator failure compensation-based command filtered control of electro-hydraulic system with position constraint, ISA Transactions, 2023, 134, 561–572. https://doi.org/10.1016/j.isatra.2022.08.023
4. Zhang F.Z.J., Cheng M., Ding R., Xu B., and Zong H. Parameter identification of hydraulic manipulators considering physical feasibility and control stability, IEEE Transactions on Industrial Electronics, 2023, 71(1), 718–728. https://doi.org/10.1109/TIE.2023.3250753
5. Pyrhönen L., Jaiswal S. and Mikkola A. Mass estimation of a simple hydraulic crane using discrete extended Kalman filter and inverse dynamics for online identification, Nonlinear Dynamics, 2023, 111(23), 21487–21506. https://doi.org/10.1007/s11071-023-08946-1
6. Yue Y., Li Y. and Zuo X. Optimization of subsea production control system layout considering hydraulic fluid pressure loss, Ocean Engineering, 2023, 288, 116047. https://doi.org/10.1016/j.oceaneng.2023.116047
7. Kumar P., Park S., Zhang Y., Jo S.H., Kim H.S. and Kim T. A review of hydraulic cylinder faults, diagnostics, and prognostics, International Journal of Precision Engineering and Manufacturing - Green Technology, 2024, 11, 1637–1661. https://doi.org/10.1007/s40684-024-00639-3
8. Prakash J., Miglani A. and Kankar P.K. Internal leakage detection in hydraulic pump using model-agnostic feature ranking and ensemble classifiers, Journal of Computing and Information Science in Engineering, 2023, 23(4). https://doi.org/10.1115/1.4056365

9. Coskun M.Y. and İtik M. Intelligent PID control of an industrial electro-hydraulic system, ISA Transactions, 2023, 139, 484–498. https://doi.org/10.1016/j.isatra.2023.04.005
10. Çetin Ş. and Akkaya A.V. Simulation and hybrid fuzzy-PID control for positioning of a hydraulic system, Nonlinear Dynamics, 2010, 61(3), 465–476. https://doi.org/10.1007/s11071-010-9662-1
11. Alleyne A. and Liu R. A simplified approach to force control for electro-hydraulic systems, Control Engineering Practice, 2000, 8(12), 1347–1356. https://doi.org/10.1016/S0967-0661(00)00081-2
12. Kalyoncu M. and Haydim M. Mathematical modelling and fuzzy logic based position control of an electrohydraulic servosystem with internal leakage, Mechatronics, 2009, 19(6), 847–858. https://doi.org/10.1016/j.mechatronics.2009.04.010
13. Liu Z., Sun J., Yue D., Zuo X., Gao H. and Feng K. A review on integral evolution of electro-hydraulic actuation in three momentous domains: aerospace, engineering machinery, and robotics, 4th Int. Conf. on Mechanical Engineering, Intelligent Manufacturing and Automation Technology, Guilin, China, 2023. https://doi.org/10.1117/12.3026210
14. Goljat S., Lovrec D. and Tič V. Advantages of pump controlled electro hydraulic actuators, Lecture Notes in Networks and Systems, 2021, 233, 774–780. https://doi.org/10.1007/978-3-030-75275-0_85
15. Quan Z., Quan L. and Zhang J., Review of energy efficient direct pump controlled cylinder electro-hydraulic technology, Renewable and Sustainable Energy Reviews, 2014, 35, 336–346. https://doi.org/10.1016/j.rser.2014.04.036
16. Casoli P., Scolari F., Vescovini C.M. and Rundo M. Energy comparison between a load sensing system and electro-hydraulic solutions applied to a 9-ton excavator, Energies, 2022, 15(7), 2583. https://doi.org/10.3390/en15072583
17. Fallahi M., Zareinejad M., Baghestan K., Tivay A., Rezaei S.M. and Abdullah A. Precise position control of an electro-hydraulic servo system via robust linear approximation, ISA Transactions, 2018, 80, 503–512. https://doi.org/10.1016/j.isatra.2018.06.002
18. Phan V.D., Vo C.P., Dao H.V. and Ahn K.K. Robust fault-tolerant control of an electro-hydraulic actuator with a novel nonlinear unknown input observer, IEEE Access, 2021, 9, 30750–30760. https://doi.org/10.1109/ACCESS.2021.3059947
19. Przystupa K. Tuning of PID controllers – approximate methods. Advances in Science and Technology Research Journal. 2018; 12(4): 56–64. https://doi.org/10.12913/22998624/99987
20. Izci D., Ekinci S. and Hussien A.G. Effective PID controller design using a novel hybrid algorithm for high order systems, PLoS One, 2023, 18(5), e0286060. https://doi.org/10.1371/journal.pone.0286060
21. Guo Y. and Mohamed M.E.A. Speed control of direct current motor using ANFIS based hybrid P-I-D configuration controller, IEEE Access, 2020, 8, 125638–125647. https://doi.org/10.1109/ACCESS.2020.3007615
22. Liem D.T. and Ahn K.K. DC motor parameters identification and sensorless torque estimation using Fuzzy PID, 12th International Conference on Control, Automation and Systems, 2012, 76–81.
23. Park D, Le T.L, Quynh N.V., Long N.K. and Hong S.K. Online tuning of PID controller using a multilayer fuzzy neural network design for quadcopter attitude tracking control, front. Neurorobot. 2021, 14, 619350. https://doi.org/10.3389/fnbot.2020.619350
24. Liem, D.T. Trajectory control of a hydraulic system using intelligent control approach based on adaptive prediction model, IFAC Journal of Systems and Control, 2023, 26, 100228. https://doi.org/10.1016/j.ifacsc.2023.100228
25. García-Martínez J.R., Cruz-Miguel E.E., Carrillo-Serrano R.V., Mendoza-Mondragón F., Toledano-Ayala M. and Rodríguez-Reséndiz J. A PID-type fuzzy logic controller-based approach for motion control applications, Sensors, 2020, 20(18), 5323. https://doi.org/10.3390/s20185323
26. Liem D.T., Truong D.Q. and Ahn K.K. A torque estimator using online tuning grey fuzzy PID for applications to torque-sensorless control of DC motors, Mechatronics, 2015, 26, 45–63. https://doi.org/10.1016/j.mechatronics.2015.01.004
27. Gupta K. Intelligent machining of shape memory alloys. Advances in Science and Technology Research Journal. 2021; 15(3): 43–53. doi:10.12913/22998624/138303
28. Vassilyev S.N., Kudinov Y.I., Pashchenko F.F., Durgaryan I.S., Kelina A.Y., Kudinov I.Y. and Pashchenko A.F. Intelligent control systems and fuzzy controllers. II. Trained Fuzzy Controllers, Fuzzy PID Controllers, Automation and Remote Control, 2020, 81(5), 922–934. https://doi.org/10.1134/S0005117920050112
29. Campos P.J., Coria L.N. and Cazarez-Castro N.R. Model-free design of speed tracking controller via fuzzy Lyapunov synthesis for a surface-mounted PMSM, Electrical Engineering, 2022, 104(3), 1565–1572. https://doi.org/10.1007/s00202-021-01414-2
30. Zhou W., Jiang R., Ding S., Cheng Y., Li Y. and Tao H. A novel grey prediction model for seasonal time series, Knowledge-Based Systems, 2021, 229, 107363. https://doi.org/10.1016/j.knosys.2021.107363
31. Liu S., Yang Y., Xie N. and Forrest J. New progress of Grey System Theory in the new millennium, Grey Systems: Theory and Application, 2016, 6(1), 2–31. https://doi.org/10.1108/GS-09-2015-0054